

1 Introduction

1.1 Classification of oscillatory fluid systems via linear stability

The transition from one flow state to another with the appearance of new patterns and unsteadiness is ubiquitous in fluid mechanics. A few representative examples of interesting oscillatory flows are shown in figure 1.1, namely (a,b) the famous von Kármán vortex street, which manifests in the wake of bluff bodies when the flow advection is sufficiently high, (c,d) a laminar-to-turbulent transition in jet flowing out of a circular nozzle and (e) surface waves in an agitated glass of water. These examples of oscillations in fluids are not merely academic but are rather fundamentally relevant to a broad spectrum of industrial applications, e.g. in the design of turbojet nozzles (d) or in the structural and dynamical analysis of skyscrapers and tanker ships (f), for which resonant vortex- or sloshing-induced vibrations could lead to catastrophic failures.

At the core of their fluid dynamic descriptions are the Navier-Stokes equations, which are a direct consequence of mass conservation and Newton's second law applied to an incompressible volume of fluid and govern the fluid velocity and pressure fields, $(\mathbf{u}, p)^T$,

$$\frac{\partial \mathbf{u}}{\partial t} + (\mathbf{u} \cdot \nabla) \mathbf{u} = -\nabla p + \frac{1}{Re} \Delta \mathbf{u}, \quad \nabla \cdot \mathbf{u} = 0, \quad (1.1)$$

and where Re is the Reynolds number, a nondimensional number that quantifies the relative importance between flow advection and diffusion. The Navier-Stokes equations, supplemented with proper case-dependent initial and boundary conditions, have been demonstrated capable of successfully englobing and describing the interplay of multiple physical mechanisms, such as advection, dissipation, external body forces, capillary and geometrical effects, turbulence, etc., in a large variety of experiments and applications. This incredible complexity often complicates the understanding of the individual physical mechanisms behind the transitions between different flow states and patterns and the emergence of unsteadiness.

For such reasons, one area of fluid mechanics that witnessed explosive growth at the end of the 20th century and that is still full of life is the study of hydrodynamic instabilities and the

Introduction

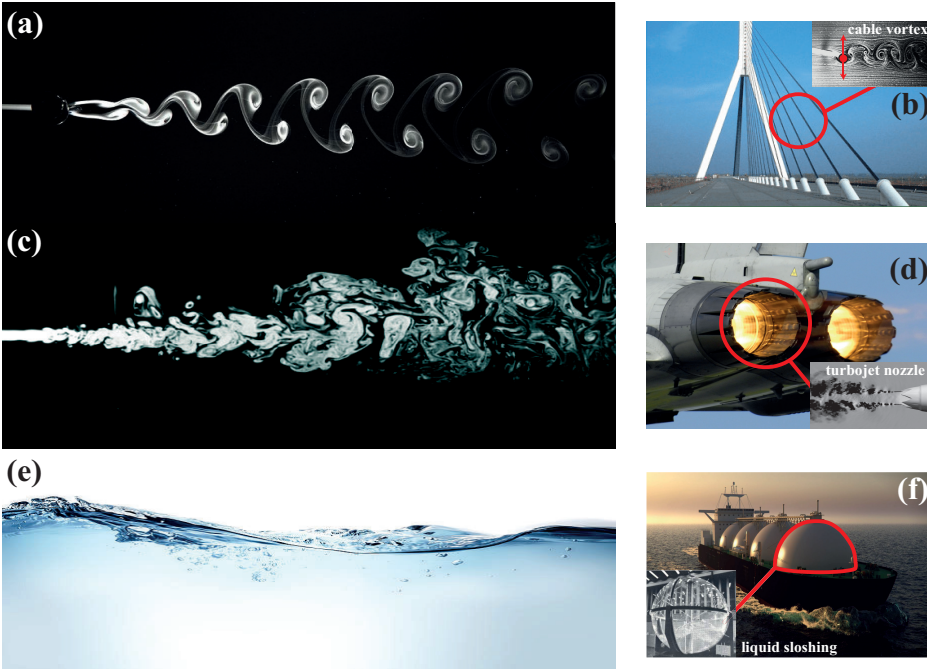


Figure 1.1 – (a) von Kármán vortex street behind a circular solid cylinder (photograph by Jürgen Wagner: https://commons.wikimedia.org/wiki/File:Karmansche_Wirbelstr_kleine_Re.JPG) and (b) around industrial cylindrical cables (inset from Seyed-Aghazadeh et al. (2021)). (c) Smoke visualisation of a jet flow (Huck, 2017) with industrial application in turbojets (d) (<https://defencyclopedia.com/2015/05/13/explained-how-jet-engines-work/>). (e) Snapshot of sloshing waves in a partially filled container with important applications in liquid transport, i.e., tanker ships' safety (f) (Credit: alexyz3d/AdobeStock) (inset from Pastoor et al. (2005)).

associated nonlinear phenomena, through linear stability and asymptotic theories.

Stability theory is indisputably the most classical approach to describe instability and state transitions, e.g. steady-to-unsteady, through bifurcations (Charru, 2011; Chomaz, 2005; Drazin and Reid, 2004; Huerre and Monkewitz, 1990; Huerre and Rossi, 1998; Schmid et al., 2002; Theofilis, 2011). The regime transition affecting a flow when a control parameter, such as Re , is varied, can be investigated by computing the linear stability of a base flow, $\mathbf{q}_0 = (\mathbf{u}_0, p_0)^T$, representing an equilibrium solution of (1.1) for fixed control parameters, to infinitesimal time-dependent perturbations, i.e. $\mathbf{q}_1 = (\mathbf{u}_1, p_1)$, such that the total flow is decomposed as $\mathbf{q} = \mathbf{q}_0 + \mathbf{q}_1$, with $\|\mathbf{q}_1\| \ll \|\mathbf{q}_0\|$. After introducing this flow decomposition in (1.1) and, successively, discretizing the linearized system of governing equations into an algebraic system, one can adopt the formalism of the *dynamical system theory* so as to write down the linearised Navier-Stokes equations in a compact form as

$$\mathcal{M} \frac{d\mathbf{q}_1}{dt} = \mathcal{L}\mathbf{q}_1, \quad (1.2)$$

where \mathcal{M} is a mass matrix and the linearized Navier-Stokes operator \mathcal{L} depends on the equilibrium state \mathbf{q}_0 computed for a fixed Re .

1.1. Classification of oscillatory fluid systems via linear stability

One can seek a linear eigensolution of (1.2) in the standard normal form $\mathbf{q}_1 = \hat{\mathbf{q}}_{1n}(\mathbf{x}) e^{(\sigma_n + i\omega_n)t}$, where the natural mode $\hat{\mathbf{q}}_{1n}(\mathbf{x})$ and its associated eigenvalue $\lambda_n = \sigma_n + i\omega_n$, are eigensolutions of the generalized eigenvalue problem

$$\lambda_n \mathcal{M} \hat{\mathbf{q}}_{1n} = \mathcal{L} \hat{\mathbf{q}}_{1n}. \quad (1.3)$$

Let us suppose that at some threshold value, e.g., of the Reynolds number, $Re = Re_{cr}$, the system becomes unstable to infinitesimal perturbations with growth rate, $\sigma_n = 0$, and frequency, ω_n . This is, for instance, the case of the cylinder flow of figure 1.2(a). Then, linear stability analysis will predict the exact value of $Re = Re_{cr}$ at which the instability first manifests. As for $Re > Re_{cr}$ the growth rate is positive, $\sigma_n > 0$, we expect the unstable infinitesimal perturbation (eigenmode) $\hat{\mathbf{q}}_{1n}$ to grow exponentially in time until the system progressively evolves towards a limit cycle with a large-time finite perturbation amplitude saturated by nonlinear effects, as depicted in figure 1.2(b). Moreover, if the value of ω_n at Re_{cr} differs from zero as in the cylinder flow, then the instability is oscillatory and a steady-to-unsteady regime transition occurs in the flow via a Hopf bifurcation (Jackson, 1987; Provansal et al., 1987; von Kármán, 1921; Williamson, 1988), found to be supercritical in this case (see figure 1.2(c)).

In the following, three archetypal flow problems are used to categorised unsteady oscillatory flows into three main families, namely oscillators, amplifiers and resonators, on the basis of the stability properties of their corresponding linearized Navier-Stokes operator, \mathcal{L} .

We will use ω_n to denote a natural frequency of the system, ω to indicate the actual frequency of the nonlinear system's response, whereas $\Omega = 2\pi/T$ will refer to an external driving frequency of oscillation period T .

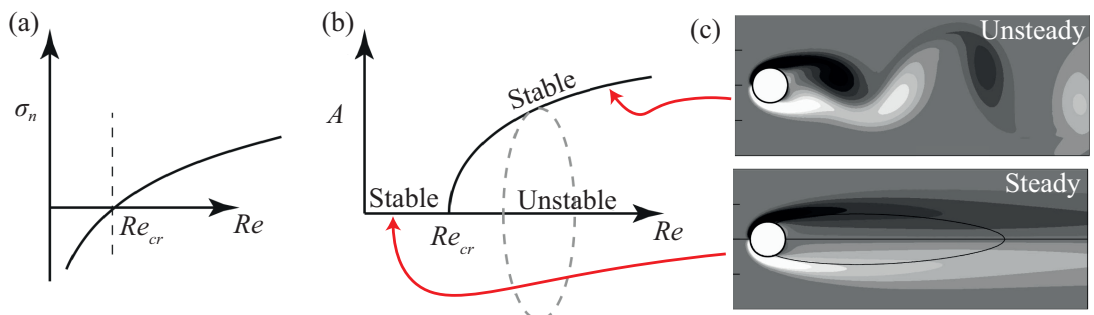


Figure 1.2 – Sketch of the supercritical Hopf bifurcation and steady-to-unsteady state transition in the cylinder flow (modified figure from (Mantić-Lugo, 2015)). (a) Sketch of the transition from stable to unstable given by a positive growth rate σ_n at the critical Reynolds number Re_{cr} . (b) Sketch of the evolution with Reynolds number Re of the saturated finite amplitude A of the periodic fluctuations, which is modelled by the Stuart-Landau amplitude equation (Stuart, 1960). (c) Flow visualization of the steady base flow (*bottom*) and a time-snapshot of the unsteady oscillatory regime for $Re > Re_{cr}$ (*top*).

Introduction

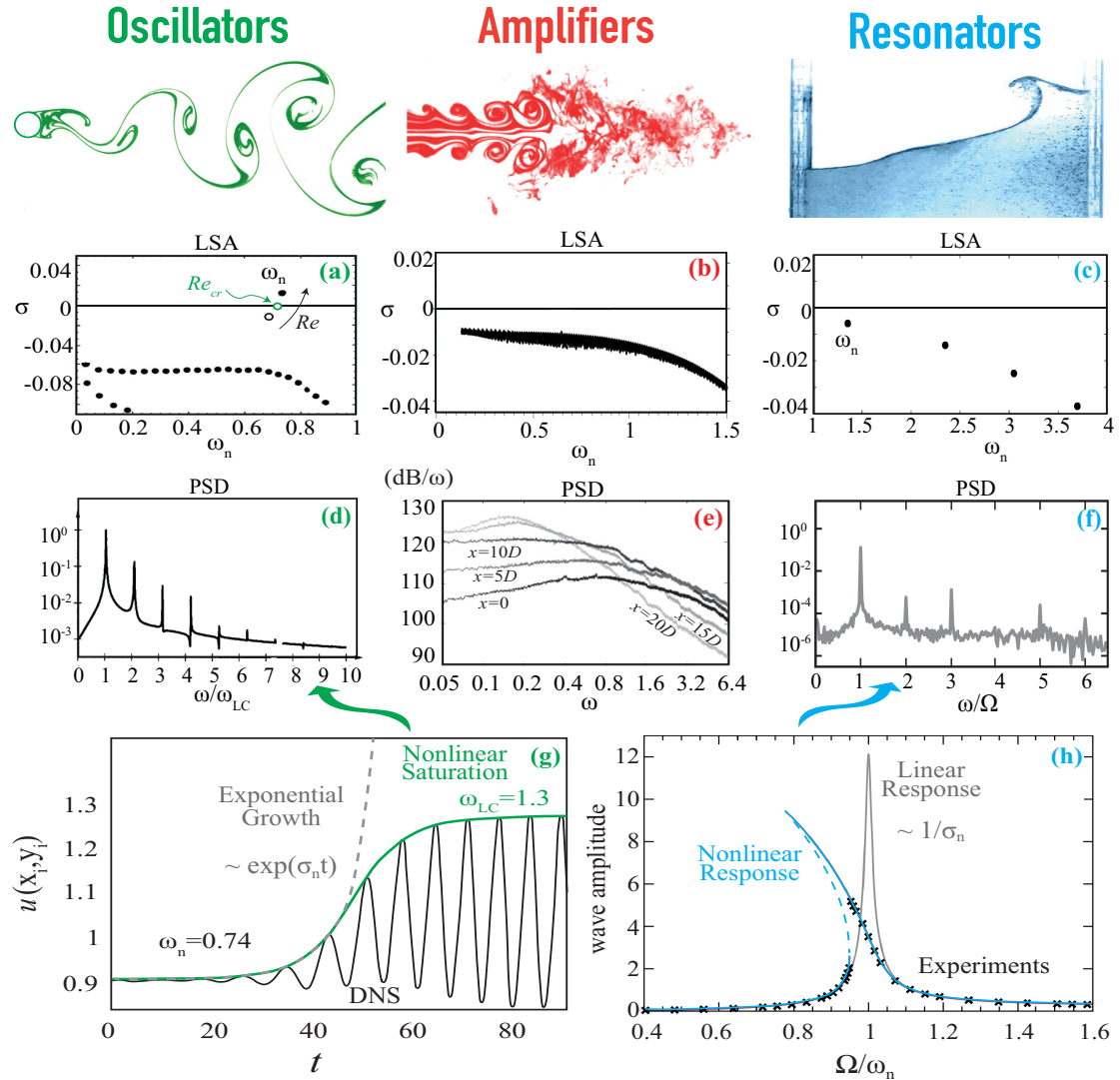


Figure 1.3 – Oscillators: cylinder flow at $Re = 140$ (figure modified from Dyke (1982)); (a) linear stability analysis (LSA) of an unstable base-flow ($Re > Re_{cr}$) in the cylinder flow showing an eigenvalue spectrum with a single unstable mode of natural frequency ω_n ; (d) Power spectral density function (PSD) extracted from a signal in the cylinder wake, showing a clear peaked frequency associated with the von Kàrmàn vortex street (Pier, 2002); (g) Time-dependent and local signal of the horizontal velocity extracted from a DNS of the cylinder flow at $Re = 100$ (Mantić-Lugo, 2015), showing the initial exponential growth, $\sim \exp(\sigma_n t)$, as well as the finite-amplitude saturation to a limit cycle with oscillation frequency $\omega_{LC} \neq \omega_n$. **Amplifiers:** turbulent jet at $Re = 10000$ (from Dyke (1982)); (b) LSA on the mean flow of a turbulent jet displaying a flat, stable spectrum (Nichols and Lele, 2010); (e) PSD of signals extracted at various streamwise locations x in a turbulent jet and showing a broad frequency response to noise (Bogey et al., 2007). **Resonators:** sloshing waves in a rectangular cell (Bäuerlein and Avila, 2021); (c) linear spectrum displaying a series of discrete and slightly damped eigenmodes; (f) PSD experimentally measured for a longitudinal time-periodic container motion of frequency Ω and showing a main peak at $\omega/\Omega = 1$; (h) The linear response peaks around $\Omega \approx \omega_n$ with an amplification $\propto 1/\sigma_n$. The nonlinear response saturates at lower values and bends the resonance curve, a feature successfully modelled by the Duffing equation (Duffing, 1918).

1.1. Classification of oscillatory fluid systems via linear stability

1.1.1 Oscillators

Figure 1.3(a) shows the eigenvalue spectrum obtained by performing the linear stability analysis (LSA) of a base-state for the famous cylinder flow, already discussed at the end of the previous section. The spectrum at $Re > Re_{cr}$ displays a well-isolated eigenvalue with natural oscillation frequency ω_n and with a positive growth rate σ_n , meaning that the equilibrium (steady) solution considered, \mathbf{q}_0 , is unstable. When looking at the power spectral density (PSD) of a time series extracted from a nonlinear flow field experimentally or numerically computed (see figure 1.3(d)), a dominant and clear peaked frequency associated with the von Kármán vortex street, together with a few higher-order harmonics of lower PSD, is well identifiable. This is a consequence of the presence of an “outstanding” eigenvalue that dictates the long-term behaviour of an initial small perturbation. More precisely, the unstable eigenmode and eigenvalue of \mathcal{L} describe the initial structure and growth of the perturbation (Theofilis, 2011) before its amplitude becomes too big and nonlinear interactions come into play (Barkley, 2006; Sipp and Lebedev, 2007). If the natural frequency, ω_n , differs from zero, as in figure 1.3(a), the flow becomes unsteady and oscillates spontaneously in a self-sustained manner. For this reason, unstable flows are typically referred to as oscillators (Huerre and Rossi, 1998).

Although oscillations naturally emerge without the need for external driving, the latter can be applied for control strategies. For instance, in certain cases, the vortex-shedding phenomenon can cause concerning structural vibrations and drag increases (Choi et al., 2008). When dealing with fluid-induced vibration issues, it’s crucial to note that unstable flow frequencies can only really become hazardous when they align with the structural modes. Therefore, adjusting the flow’s frequency slightly could be a viable solution to resolve the problem. This can be achieved in open-loop control by imposing to the unstable flow an external harmonic forcing of frequency Ω , amplitude f and with a proper spatial structure, $\mathbf{q}_f(\mathbf{x})$ (Sipp, 2012). Indeed, if the forcing frequency Ω is chosen close to the natural frequency ω_n , then the flow oscillations will lock onto Ω , so as to shift the frequency and move it away from the resonance (see Fauve (1998), Bender et al. (1999) and Chapter 8 of Charru (2011) for further details on the lock-in phenomenon).

1.1.2 Amplifiers

In figure 1.3(b) we report the eigenvalue spectrum of an amplifier flow, i.e. a laminar jet of air flows exiting a circular tube and whose edges, moving downstream, develop axisymmetric oscillations, rolls up into vortex rings, and then abruptly becomes turbulent. Despite the fact that the eigenvalue-spectrum is fully stable, the PSD function of a local time-series in the jet flow, reported figure 1.3(e), shows that small harmonic external excitations result in a large amplification of the system responses (Crow and Champagne, 1971). Moreover, the system response has a rather broad or mildly selective frequency selection mechanism, with a frequency of maximum amplification which does not necessarily match one of the least stable modes. These features can be better understood by drawing attention to the non-normality of the linear operator \mathcal{L} . A linear operator \mathcal{L} is said to be non-normal if it does not commute

Introduction

with its adjoint operator, \mathcal{L}^\dagger , i.e. $\mathcal{L}\mathcal{L}^\dagger \neq \mathcal{L}^\dagger\mathcal{L}$. It is important to note that the definition of the adjoint operator is not univocal, but rather depends on the introduction of an arbitrary inner product, although the latter is very often chosen so as to represent an energy norm for the system, e.g. the total or kinetic energy. If the operator is non-normal, the eigenmode basis is not orthogonal. It follows that, even for a stable operator, whose eigenmodes all decay at large times, small initial perturbations may experience very large transient growth. Strong non-normality also possibly implies high sensitivity to small operator perturbations and a large response to harmonic forcing away from eigenfrequencies (Ducimetière et al., 2022a,b; Trefethen et al., 1993), hence arguing for the importance of sensitivity analysis and flow control of these systems (Bottaro et al., 2003; Boujo and Gallaire, 2015; Camarri, 2015; Sipp et al., 2010). In the case of the Navier-Stokes operator, non-normality is generally produced by strong streamwise advection of the base flow (Chomaz, 2005; Farrell and Ioannou, 1996; Schmid, 2007; Schmid et al., 2002; Trefethen et al., 1993). Therefore, the linear stability analysis, capable of predicting the instability onset in oscillators with a dominant unstable eigenmode, appears almost irrelevant in these scenarios and it thus fails in describing the dynamics of strongly non-normal flows like noise amplifiers.

1.1.3 Resonators

An example of a resonator is represented by sloshing, a term used to denote any motion of the free liquid surface in a partially filled reservoir subjected to horizontal motions, i.e. perpendicular to the direction of gravity. Figure 1.3(c) shows the eigenvalue spectrum of a typical sloshing system. The eigenvalues correspond to the natural sloshing modes, i.e. free surface capillary-gravity waves, for a container, e.g. rectangular, partially filled with a liquid and undergoing a longitudinal harmonic motion at a driving frequency $\Omega = 2\pi/T$ (see also figure 1.4). In absence of external forcing, the equilibrium or base-state configuration for this flow is a liquid column stably at rest under the effect of gravity. Thus, similarly to the amplifier system of figure 1.3(b), the linear spectrum is stable, although the eigenvalues are here well separated from each other, as a result of the lateral confinement, which, through necessary boundary conditions, only allows for some specific modal perturbations (Faltinsen and Timokha, 2009; Ibrahim, 2005). In our classification, what fundamentally discerns resonators from amplifiers is the normal nature of the linearized Navier-Stokes operator. Indeed, for resonators like that of figure 1.3, the linearized operator \mathcal{L} is typically normal, meaning that it commutes with its adjoint (Viola et al., 2018; Viola and Gallaire, 2018), i.e. $\mathcal{L}\mathcal{L}^\dagger = \mathcal{L}^\dagger\mathcal{L}$ (and \mathcal{L} is said to be self-adjoint). As a consequence, the eigenmode basis is fully orthogonal. These features have strong implications for the system's response to perturbations and harmonic forcing in resonators. Given the stability and self-adjointness of \mathcal{L} , the linear evolution of initial perturbations, which is given by the superposition of eigenvectors, shows a decaying large-time behaviour without experiencing any transient growth. Furthermore, a sustained oscillatory response can only be achieved by externally driving the system, e.g. at a forcing frequency Ω . If the system is subjected to white noise or, more simply, to a harmonic forcing of varying frequency Ω , the maximum amplification is achieved in the neighbourhood of a

1.1. Classification of oscillatory fluid systems via linear stability

natural frequency, i.e. for $\Omega \approx \omega_n$, with a linear amplitude response $\sim 1/\sigma_n$ (see figure 1.3(h)), hence showing a very precise frequency selection mechanism, in contradistinction with the broad frequency response of amplifiers.

Within the family of resonators, we can further distinguish among three sub-classes of oscillatory responses depending on their nature, namely driven oscillations, parametric oscillations and natural transient oscillations resulting from a non-zero initial condition.

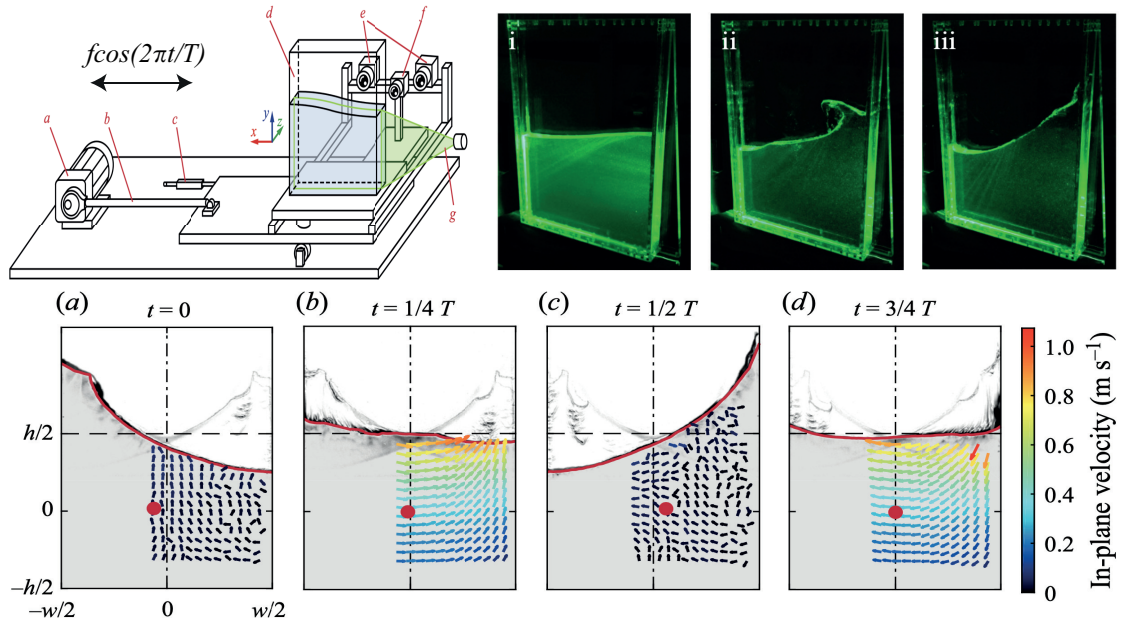


Figure 1.4 – *Top:* A sketch of the experimental apparatus of Bäuerlein and Avila (2021) and snapshots of different sloshing states observed. *Bottom:* Sloshing liquid in a horizontally oscillated rectangular tank over one oscillation period (Bäuerlein and Avila, 2021). The tank has a width of $w = 500$ mm, is filled with water to the height $h = 400$ mm and is driven with the frequency $\Omega = 2\pi/T$, with $T = 0.88$ s ($1/T = 1.13$ Hz). Nonlinear resonances amplify periodic surface waves (marked as a red line) and produce oscillations of the liquid's centre of mass (indicated by red circles). Stereoscopic particle image velocimetry measurements of the in-plane velocity (displayed as arrows) show that the maximum velocities are reached when the surface elevation is lowest. The excitation frequency is close to the first system's natural frequency resonance, $\Omega/\omega_n = 0.917$ (harmonic resonance). The excitation amplitude is $f = a\Omega^2$, with $a = a_x/w = 0.64$ (a_x is the peak amplitude of the horizontal tank displacement).

Driven oscillations

When a resonator like the sloshing system of figures 1.3 and 1.4 is externally driven at a frequency Ω , the large-time response is generally characterized by a finite amplitude, set by the saturation resulting from the system's dissipation and nonlinear mechanisms, and by an oscillation frequency coinciding with that of the external forcing. Indeed, the PSD function shows a main peak centred around $\omega/\Omega \approx 1$ and a series of super-harmonics triggered by

Introduction

nonlinear effects. The PSD function of figure 1.3(f) is reminiscent of that typical of oscillators (see figure 1.3(d)), although here, oscillations are not self-sustained but are rather maintained by the external driving.

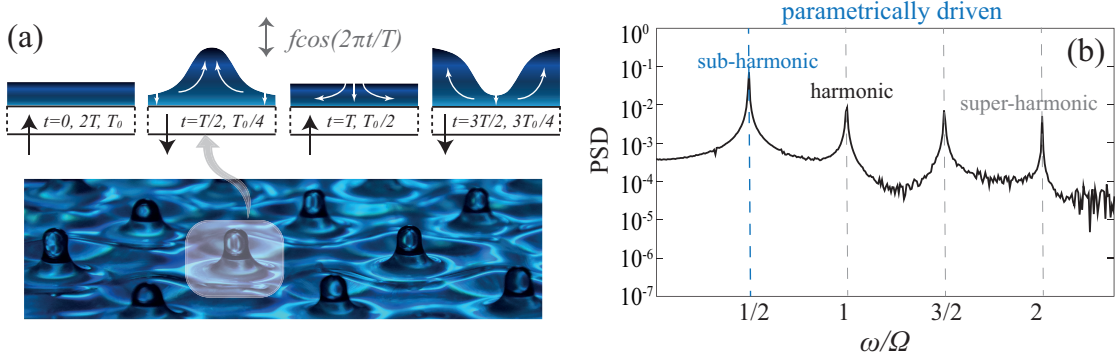


Figure 1.5 – (a) A vertically vibrating liquid layer that spontaneously excites sub-harmonic surface standing waves (Benjamin and Ursell, 1954; Faraday, 1831; Kumar and Tuckerman, 1994a) (modified figure from Sampara and Gilet (2016)). (b) Power spectral density (PSD) computed numerically by simulating the response of a liquid layer in a cylindrical container vertically excited at a frequency Ω (Bongarzone et al., 2021b). The PSD shows a dominant peak at $\omega/\Omega = 1/2$, thus indicating a sub-harmonic parametric response.

Parametric oscillations

Parametric resonators are systems where an oscillatory system's response can be induced by time-modulating one or more internal parameters of the system at some frequencies that possibly differ from its natural frequencies, $\Omega \neq \omega_n$. Such a modulation can be achieved in several ways; a simple archetypal example is given by the parametric pendulum, whose pivot position is vertically modulated by imposing an external forcing. This translates into a modulation of the gravity acceleration acting on the system, which can then be parametrically and resonantly pumped by frequency modulations with $\omega_n/\Omega \approx p/2$ ($p \in N$) (Kovacic et al., 2018a). The strongest amplification is typically achieved for $\omega_n/\Omega \approx 1/2$, and it is referred to as sub-harmonic resonance. This parametric amplification also occurs in continuous media. For instance, the flat interface of a liquid contained in a vertically vibrating tank (see figure 1.5(a)) may be parametrically excited, leading to the generation of standing waves oscillating at a frequency (see figure 1.5(b)) that is half that of the external driving, leading to the so-called Faraday instability (Benjamin and Ursell, 1954; Faraday, 1831; Kuhlmann and Rath, 1998; Kumar and Tuckerman, 1994a).

Since the two examples of parametric oscillations mentioned here both involve the use of an external forcing, the distinction between driven and parametric resonators may still appear somewhat vague at this stage. Nevertheless, such a distinction becomes much clearer at the level of the governing equations, particularly by noticing that, while the external forcing in driven resonators appears as an additive extra term, in parametric resonators the forcing is multiplicative and it appears in front of one or more state variables. Explicative archetypal

1.1. Classification of oscillatory fluid systems via linear stability

examples of this differentiation are offered in the following by the Duffing equation (1.7) (driven) and by the Mathieu equation (1.15).

Natural oscillations

If, for instance, the external driving is eventually turned off as in figure 1.6(b), the stable nature of these resonators no more allows for sustained oscillations and the system enters a new dynamical phase during which it relaxes towards the original equilibrium solution through natural, free, oscillations. The amplitude response decreases with time and the system, initially oscillating at the driving frequency Ω , progressively adjusts its free oscillation frequency, which will tend to the least damped natural frequency ω_n at large times. The relaxation dynamics is ideally exponential with a decay rate possibly dictated by the damping rate of the least damped natural mode, i.e. $\sim \exp(\sigma_n t)$ ($\sigma_n < 0$), although nonlinear phenomena, such as friction or free surface and contact line capillary effects in confined liquid oscillations (see figure 1.6(a) and Viola (2016)), becoming more and more important as the wave amplitude decreases, may alter the features of the decaying behaviour. As a side comment, we note that, in order to observe the natural evolution dynamics, the system does not necessarily have to start from sustained oscillations; it could start from any initial condition, e.g. an impulsive perturbation.

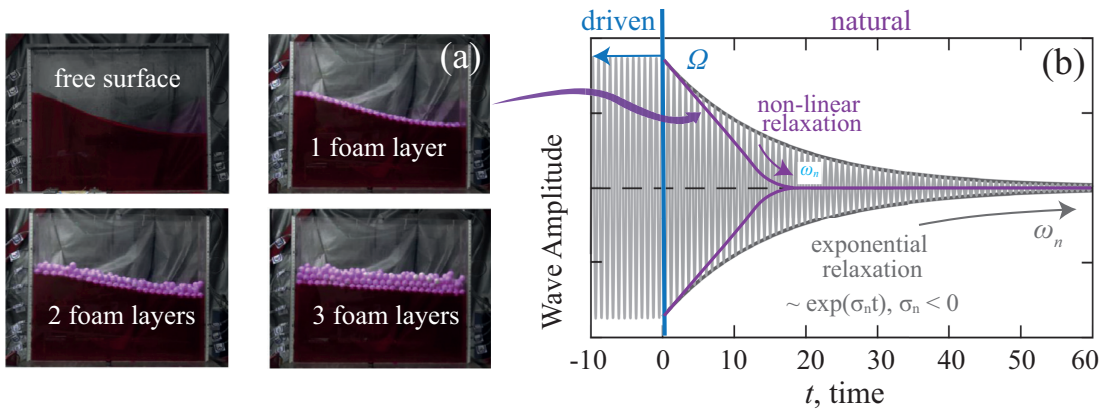


Figure 1.6 – (a) Nonlinear friction in sloshing dynamics is induced by one or more layers of foam placed at the free surface (Zhang et al., 2019). As a consequence, the sloshing wave does not relax exponentially (Sauret et al., 2015; Viola et al., 2016c). (b) Relaxation dynamics of a harmonically driven sloshing wave following the suppression of the external driving at time $t = 0$ (modified figure from Bäuerlein and Avila (2021)). In the absence of nonlinear effects, the relaxation dynamics is exponential, with a decay rate defined by the damping coefficient σ_n of the previously excited natural mode. However, nonlinear friction acting at the contact line may affect the relaxation dynamics provoking the motion arrest at finite times (Coccia et al., 1993; Dollet et al., 2020; Viola et al., 2018) (see purple line in connection with panel (a)). In both scenarios, the system, initially oscillating non-parametrically at the driving frequency Ω , progressively adjusts its oscillation frequency, which equals the natural frequency ω_n at large times.

1.2 Nonlinear effects and envelope equations

The physical problems investigated in this thesis are all attributable to the two categories of oscillators and resonators, for which linear stability analysis provides relevant and useful pieces of information about the initial evolution of a perturbation and the response to weak external forcing. Nevertheless, even when non-normal effects are not important or completely absent, as for most of the oscillators and resonators, the linear modal behaviour, used for the classification outlined in the previous section, does not always fully capture the entire dynamics of the perturbation.

In figure 1.3(g) and (h), we have already anticipated the role that nonlinearities play in the cylinder flow and for resonantly driven sloshing waves in a rectangular container. For instance, in an unstable cylinder flow, i.e. $Re > Re_{cr}$, the perturbation, initially oscillating at the natural frequency ω_n , grows exponentially until the amplitude becomes large enough and nonlinear mechanisms kick in. The oscillation frequency progressively increases, while the perturbation amplitude saturates and the system eventually settles into a limit cycle, with self-sustained oscillations at $\omega = \omega_{LC} \neq \omega_n$ and finite amplitude. The amplitude saturation and the frequency modulation are direct consequences of nonlinear mechanisms. Similar saturation and frequency detuning effects, as well as other nonlinear effects, happen in sloshing and Faraday waves, although the wave motion needs to be triggered and permanently sustained by external driving. We have also shown, in figure 1.6, how some kind of nonlinear effects (sub-linear (Viola, 2016)), such as capillary-induced friction in confined surface waves, can nonlinearly damp the oscillations and, becoming particularly effective at small amplitudes, eventually induce the arrest of the interface motion at finite times.

Generally speaking, a high-fidelity description and prediction of nonlinear phenomena observed in real-life experiments are only achievable by solving the fully nonlinear governing equations, which often do not admit closed-form analytical solutions. Accurate approximated solutions can be computed via direct numerical simulations (DNS), which are, however, computationally costly. Hence, the formalization of reduced models involving lower degrees-of-freedom, such as envelope (also called amplitude) equations, derived by means of asymptotic theories and englobing the relevant nonlinear flow features, constitutes an attractive alternative to DNS whenever applicable, e.g. when nonlinear effects are only weak. With regards to oscillators and resonators, nonlinearities are generally small close to bifurcation points and for small external forcing amplitudes.

For example, Provansal et al. (1987) and Dušek et al. (1994) observed that, in the case of the first instability in the cylinder wake, the complex amplitude of the perturbation, $A = |A|e^{i\Phi}$, close to the bifurcation ($Re \approx Re_{cr}$) is governed by the Stuart-Landau equation (Stuart, 1960),

$$\boxed{\frac{dA}{dt} = \lambda A + \nu |A|^2 A}, \quad (1.4)$$

which describes the saturation mechanism in this super-critical Hopf bifurcations (Kuznetsov et al., 1998) (see figure 1.2(b)) as the steady base flow passes from stable to unstable, providing an estimation of the time evolution of the instability amplitude.

1.2. Nonlinear effects and envelope equations

The complex coefficients $\lambda = \lambda_r + i\lambda_i$ and $\nu = \nu_r + i\nu_i$, originally determined experimentally, have been computed in a rigorous manner by Sipp and Lebedev (2007) using weakly nonlinear analysis for the Navier-Stokes equations in the neighbourhood of the critical Reynolds number, Re_{cr} (Stuart, 1958). They showed that the Stuart-Landau equation naturally appears as a compatibility condition in the asymptotic scheme. In the same spirit, a weakly nonlinear mode expansion for different flows (precessing vortex breakdown, wakes of disks and spheres) has been carried out by Meliga et al. (2009a, 2012a).

At the core of these perturbative analyses is the multiple-scales method (Cole, 1968), which has been widely used to obtain amplitude equations describing the slow dynamics of the large-scale modulation of a basic structure predetermined by *a-priori* calculations, e.g. from global or local linear stability (Newell and Whitehead, 1969; Segel, 1969). The method lies within the family of asymptotic techniques and it assumes, after non-dimensionalization of the governing equations, the existence of a small non-dimensional parameter $\epsilon \ll 1$ in the underlying problem and that can be taken, for instance, as a measure of the departure from criticality in terms of control parameters, e.g. $Re^{-1} - Re_{cr}^{-1} \sim \epsilon$, or as the amplitude of a small external forcing, $f \sim \epsilon$, if any. It is then meaningful to seek for a solution \mathbf{q} as a formal power series in the small parameter, i.e. $\mathbf{q} = \mathbf{q}_0 + \epsilon \mathbf{q}_1 + \epsilon^2 \mathbf{q}_2 + \dots + \epsilon^k \mathbf{q}_k + O(\epsilon^{k+1})$, where in most cases, retaining only the first few terms of the series is sufficient to describe the small ϵ behaviour of the actual solution. In fact, the multiple scales approach consists in postulating that the system's functions vary on two (or more) temporal and/or spatial scales, so that some functions, e.g. the perturbation amplitude, depend on time t and space \mathbf{x} , only through the product $T_i = \epsilon^i t$ and $X_j = \epsilon^j \mathbf{x}$, e.g. $A(\epsilon t, \dots, \epsilon^i t, \epsilon \mathbf{x}, \dots, \epsilon^j \mathbf{x}) = A(T_1, \dots, T_i, \mathbf{X}_1, \dots, \mathbf{X}_j)$, with $i, j < n$. Requiring, through the imposition of a solvability condition, the suppression of unphysical secular terms in the standard expansion eventually fixes the ensuing arbitrariness by providing a governing equation for A .

As a more general example, the combined introduction of slow time and spatial scales is the starting point in the derivation of the famous nonlinear Schrödinger equation (NLS) (Ablowitz et al., 1991; Benjamin and Feir, 1967; Stoker, 1992; Whitham, 1974; Zakharov, 1972), as an envelope equation for gravity waves that describes the evolution of slowly modulated wavetrains:

$$\frac{\partial A}{\partial t} - \gamma \frac{\partial^2 A}{\partial x^2} = \nu |A|^2 A, \quad (1.5)$$

(written in a non-dimensional form and in a coordinate system moving with the group velocity) with coefficients $\gamma = -i\omega_n/8k_n^2$, $\nu = -i\omega_n k_n^2/2$ and where k_n represents the wave number of the carrier wave, whereas $\omega_n = \sqrt{gk_n}$ (g : gravity acceleration) is the linear dispersion relation of gravity waves in the deep water regime (Lamb, 1993). For instance, an important issue in naval engineering is the phenomenon of rogue waves, extreme events occurring in systems characterized by the presence of many waves (Onorato et al., 2001); most of the models which have been developed so far have a weakly nonlinear nature and are based on the NLS. See Onorato et al. (2013) for a series of representative examples, where the main physical mechanisms at the origin of rogue waves are elucidated.

The NLS appears in different physical contexts, including plasma physics and nonlinear

Introduction

optics, since it simply describes the interaction of dispersion and weak nonlinearity. Equation (1.5) is a special case of an amplitude equation for a conservative system. In the more common case where dissipation cannot be neglected, the usual amplitude equation is the so-called complex Ginzburg-Landau equation (Aranson and Kramer, 2002; Godrèche and Manneville, 1998),

$$\frac{\partial A}{\partial t} - \gamma \frac{\partial^2 A}{\partial x^2} = \lambda A + \nu |A|^2 A, \quad (1.6)$$

where coefficients γ , λ and ν are not purely imaginary as in (1.5). To give a few examples, equation (1.6) has been used to describe the Benjamin-Feir phase instabilities, as well as other symmetry-breaking secondary instabilities of cellular flows, as the Eckhaus and the “zigzag” instabilities (Godrèche and Manneville, 1998).

1.2.1 Weakly nonlinear analysis via multiple *time-scales* method

A multiple scales expansion in space is commonly employed in WKBJ approaches (Bender et al., 1999; Gaster et al., 1985; Huerre and Rossi, 1998; Nayfeh, 2008a) for weakly nonparallel flows, in which the steady base or mean flow varies slowly on a long length scale when compared to the shorter instability waves (Charru, 2011; Chomaz, 2005; Schmid et al., 2002).

However, in the problems tackled in this thesis, the effect of the geometry and confinement on the flow is such that the instabilities and the base flow have no separated length scales: the dynamics of the perturbation result from the interactions of global modes extended over the whole physical domain and whose spatial structures valid at any spatial location can be computed by means of linear stability calculations. As a result, no slow spatial scales need to be introduced, and one only needs to account for slow time modulations of the perturbation amplitudes, which are governed by nonlinear ODEs, rather than PDEs as in the case of the nonlinear Schrödinger equation (1.5) or the Ginzburg-Landau equation (1.6).

Since the weakly nonlinear analysis via multiple *time-scales* method constitutes a fundamental theoretical building block of the present work, in the following we provide a quick overview of the method, using as examples a series of archetypal single-degrees-of-freedom systems.

Asymptotic solution of the forced Duffing equation

Let us first consider the Duffing equation (Duffing, 1918), a popular single-degrees-of-freedom system often used to model the nonlinear response of externally driven resonators,

$$\ddot{x} + 2\sigma_n \dot{x} + \omega_n^2 x + \beta x^3 = f \cos \Omega t, \quad (1.7)$$

where σ_n is the damping coefficient, β is the nonlinear coefficient, while f and Ω are the driving amplitude and frequency. In the following, we only consider the limit of small forcing amplitudes, $f = \epsilon \hat{f}$, weak nonlinearities, $\beta = \epsilon \hat{\beta}$ and small damping, $\sigma_n = \epsilon \hat{\sigma}_n$, with the auxiliary parameters \hat{f} , $\hat{\beta}$ and $\hat{\sigma}_n$ assumed of order $\sim O(1)$. Most generally speaking, ϵ represents

1.2. Nonlinear effects and envelope equations

a small parameter, i.e. $0 < \epsilon \ll 1$, which does not necessarily need to be explicitly defined, but it can rather be considered as an implicit separation of the different orders of magnitude at play. A straightforward perturbation-series approach to the problem proceeds by writing $x(t) = x_0(t) + \epsilon x_1(t) + O(\epsilon^2)$ and substituting this into (1.7). Matching powers of ϵ gives the ϵ^0 -order equation

$$\ddot{x}_0 + \omega_n^2 x_0 = 0 \quad \longrightarrow \quad x_0 = A e^{i\omega_n t} + c.c., \quad (1.8)$$

with *c.c.* denoting the complex conjugate, and ϵ -order problem

$$\ddot{x}_1 + \omega_n^2 x_1 = -2\hat{\sigma}_n \dot{x}_0 - \hat{\beta} x_0^3 + \hat{f} \cos \Omega t = \frac{\hat{f}}{2} e^{i\Omega t} - 2\hat{\sigma}_n i A e^{i\omega_n t} - \hat{\beta} A^3 e^{i3\omega_n t} - 3\hat{\beta}|A|^2 A e^{i\omega_n t} + c.c., \quad (1.9)$$

$$\begin{aligned} x_1 = A^3 \frac{\hat{\beta}}{8\omega_n^2} e^{i3\omega_n t} - \left(|A|^2 \frac{3\hat{\beta}}{4\omega_n^2} + i \frac{\hat{\sigma}_n}{2\omega_n^2} \right) A e^{i\omega_n t} - \frac{\hat{f}}{\Omega^2 - \omega_n^2} e^{i\Omega t} + \\ + \underbrace{\left[i|A|^2 \frac{3\hat{\beta}}{2\omega_n} - \frac{\hat{\sigma}_n}{\omega_n} \right] A t e^{i\omega_n t}}_{\propto t} + c.c., \end{aligned} \quad (1.10)$$

where the second-order homogeneous solution in (1.10) has been omitted for brevity.

The most general solution of (1.10) is unbounded due to the linear terms in t (see framed terms in (1.10)), which are classically referred to as *secular terms*. In particular, for $t = O(\epsilon^{-1})$, these terms become $O(1)$ and have the same order of magnitude as the leading-order term, x_0 . Because the asymptotic terms have become disordered, the series is no longer an asymptotic expansion of the solution, i.e. the straightforward perturbation expansion breaks down. Such a linear growth is obviously a spurious effect since it is clear that (1.7) conserves energy. This pathological behaviour is resolved by resorting to the multiple scales framework (Godrèche and Manneville, 1998; Nayfeh, 2008a). Let us introduce explicitly the slow time scale $T = \epsilon t$, which leads to

$$\frac{d}{dt} = \frac{\partial}{\partial t} + \epsilon \frac{\partial}{\partial T} + O(\epsilon^2) \quad \frac{d^2}{dt^2} = \frac{\partial^2}{\partial t^2} + 2\epsilon \frac{\partial^2}{\partial t \partial T} + \epsilon^2 \frac{\partial^2}{\partial T^2} + O(\epsilon^3), \quad (1.11)$$

as if t and T were independent variable. With these definitions, the ϵ^0 -order problem remains unchanged and has solution $x_0 = A(T) e^{i\omega_n t} + c.c.$ The only, but fundamental, difference, consists in assuming that amplitude $A(T)$ is now a function of the slow time scale, it represents the slow wave-amplitude modulation of the fast wave oscillations, and it is still undetermined at this stage of the asymptotic expansion. The ϵ -order problem is now forced by the following terms:

$$\begin{aligned} \frac{\partial^2 x_1}{\partial t^2} + \omega_n^2 x_1 = -2 \frac{\partial^2 x_0}{\partial t \partial T} - 2\hat{\sigma}_n \frac{\partial x_0}{\partial t} - \hat{\beta} x_0^3 + \hat{f} \cos \Omega t \\ = \left(-2i\omega_n \frac{\partial A}{\partial T} - 2i\hat{\sigma}_n \omega_n A - 3\hat{\beta}|A|^2 A + \frac{\hat{f}}{2} e^{i\hat{\Lambda}T} \right) e^{i\omega_n t} + c.c. + NRT, \end{aligned} \quad (1.12)$$

Introduction

where NRT stands for non-resonating terms, meaning terms that are not secular and that are not necessarily relevant for further analysis (unless one aims at pursuing the expansion to the next order). In (1.12), we have already considered the most dangerous scenario, in which the system is driven close to the natural frequency (resonant condition). This has been done by introducing a small detuning parameter Λ , i.e. $\Omega = \omega_n + \Lambda$ with $\Lambda = \epsilon \hat{\Lambda}$ (and $\hat{\Lambda} \sim O(1)$), such that $\Omega t = \omega_n t + \hat{\Lambda} T$ in (1.12). The arbitrariness introduced by $A(T)$ is fixed by requiring that secular terms are not present in the solution (1.10), which implies cancelling out the harmonic forcing terms in ω_n appearing on the right-hand side of (1.12) or (1.9). Such a solvability condition prescribes the amplitude $A(T)$ to obey the following ordinary differential equations

$$\frac{\partial A}{\partial T} = \frac{1}{\epsilon} \frac{dA}{dt} = \hat{\lambda} A + \hat{v}|A|^2 A + \mu \hat{f} \quad \xrightarrow[\text{reintroducing the physical time } t \text{ by eliminating } \epsilon]{} \boxed{\frac{dA}{dt} = \lambda A + v|A|^2 A + \mu f}, \quad (1.13)$$

with coefficients $\lambda = \epsilon \hat{\lambda} = -(\sigma_n + i(\Omega - \omega_n))$, $v = \epsilon \hat{v} = i3\beta/2\omega_n$ and $\mu = -i/4\omega_n$ and where the transformation $A \rightarrow Ae^{i\hat{\Lambda}T}$ has been used so as to make the amplitude equation autonomous. Note that (1.13) takes the form of a Stuart-Landau equation supplemented with an external driving term. Hence, the envelope equation (1.13) provides a governing equation for the perturbation's amplitude and the leading order solution, $x_0 = A(t) e^{i(\omega_n + \Lambda)t} + c.c. = 2|A(t)| \cos(\Omega t + \Phi(t))$, represents a good approximation of (1.7) valid for small forcing in the vicinity of the resonance and for weak nonlinearities.

The close-to-resonant asymptotic approximation of the forced Duffing equation has been widely used in the modelling of resonant sloshing waves, e.g. in rectangular container (Bäuerlein and Avila, 2021; Ockendon and Ockendon, 2001, 1973), and it has been shown capable of describing the finite wave amplitude saturation through hardening- or softening-like behaviours. By properly fitting coefficients σ_n and β from experimental measurements by Bäuerlein and Avila (2021) (see also figure 1.4), the latter can be compared with the predictions from approximation (1.13). This is outlined in figure 1.7(a) in terms of non-dimensional steady-state wave amplitude (large-time dynamics) for different non-dimensional forcing amplitude. These steady-state solutions can be obtained, e.g., by time-integrating (1.13) for large time intervals. Alternatively, one can directly seek stationary solutions by setting $dA/dt = 0$ and then study their stability to small perturbations in the form $A = A_0 + \epsilon A_1 e^{(s_r + is_i)t}$, so that the sign of s_r establishes whether the steady solution A_0 is stable or unstable.

Mathieu's equation with nonlinearities

With regard to this thesis, another relevant single-degree-of-freedom system, used to model the response of parametrically driven resonators, is the parametric pendulum, already introduced in the previous section. At the linear order, this simple system is described by the Mathieu equation (Mathieu, 1868)

$$\ddot{x} + 2\sigma_n \dot{x} + \omega_n^2 x = x\omega^2 \epsilon f \cos \Omega t. \quad (1.14)$$

The parametrically unstable regions in the forcing parameter space (Ω, f) can be computed by means of the linear *Floquet* stability theory performed around one of the two possible

1.2. Nonlinear effects and envelope equations

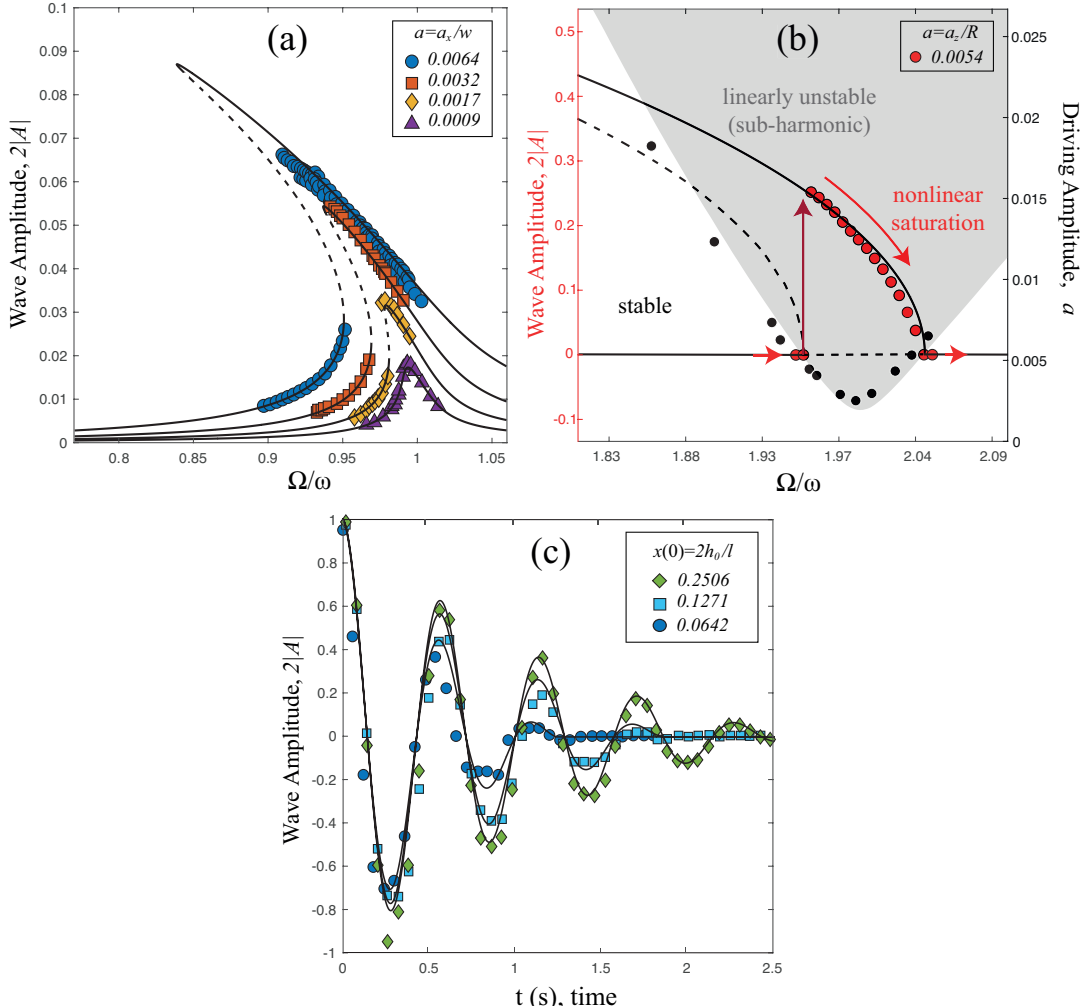


Figure 1.7 – (a) Asymptotic approximation (1.13) is compared with sloshing experiments in a rectangular container by (Bäuerlein and Avila, 2021). The comparison is outlined in terms of the non-dimensional steady-state wave amplitude (large-time dynamics) of the wave's center of mass for different non-dimensional forcing amplitude, a . Those amplitudes are re-scaled by the container's width, w (see figure 1.4). The forcing acceleration is $f = c_1 a \Omega^2$, with Ω the driving frequency and $c_1 = 0.3183$ a characteristic system parameter. Coefficients σ_n and ν are set to 8.4×10^{-3} and -59.2 , respectively. (b) Asymptotic approximation (1.16) is compared with experiments by (Henderson and Miles, 1990) for single-mode Faraday waves in a small circular cylinder. The grey-shaded area represents the sub-harmonically unstable region in the (Ω, a) forcing parameter space (right-y axis), whereas lines correspond to the nonlinear amplitude saturation (left-y axis). Amplitudes are re-scaled by the container's radius R . The forcing acceleration is $f = c_1 a \Omega^2$, with $c_1 = 1.0291$. Coefficients: $\sigma_n = 0.0157$ and $\beta = -6$. (c) Asymptotic approximation (1.18) is compared with the measurements by (Dollet et al., 2020) of the relaxation dynamics of liquid oscillations in a U-shaped tube. The amplitude is rescaled by the initial non-dimensional elevation, $2h_0/l$ with l the overall tube length. Coefficients: $\sigma_n = 0.06$ and $\Delta = 0.0047$. In (a,c), $\omega_n = 1$, while $\omega_n = 1.9641$ in (b). In (a,b,c) lines indicate the asymptotic approximations, whereas markers denote experiments. In (a,b), dashed lines designate unstable steady-state solutions of (1.13) and (1.16). In (a,b,c), parameters σ_n , β and Δ are fitted in order to match the experiments.

Introduction

equilibrium solutions (Kovacic et al., 2018a). Within such regions the equilibrium solution is unstable, and the perturbation grows exponentially. The most relevant parametric resonance is the sub-harmonic one, as it is the one that requires the lowest driving amplitude to be excited. Yet, equation (1.15) does not tell us anything about nonlinear mechanisms. Nonlinearities are partially reintroduced by accounting for a cubic term ($\sin x \approx x - x^3/6 + \dots$) (Kovacic et al., 2018a),

$$\ddot{x} + 2\sigma_n \dot{x} + \omega_n^2 x + \beta x^3 = x \omega_n^2 f \cos \Omega t. \quad (1.15)$$

Without going into the details (the derivation is similar to that for the Duffing equation), an asymptotic approximation of the fundamental sub-harmonic resonance can be obtained from (1.15) via multiple time-scales method in the limit of small forcing amplitude, $f = \epsilon \hat{f}$, weak damping, $\sigma_n = \epsilon \hat{\sigma}_n$, weak nonlinearities, $\beta = \epsilon \hat{\beta}$, and assuming a driving frequency to be $\Omega = 2\omega_n + \Lambda = 2\omega_n + \epsilon \hat{\Lambda}$, i.e. in the neighbourhood of the sub-harmonic resonance. Note that the introduced auxiliary parameter \hat{f} , $\hat{\sigma}_n$, $\hat{\beta}$ and $\hat{\Lambda}$ are all of order $\sim O(1)$. The asymptotic procedure and the imposition of a solvability condition lead to the following amplitude equation

$$\boxed{\frac{dA}{dt} = \lambda A + \nu |A|^2 A + \mu \bar{A} f}, \quad (1.16)$$

with $\lambda = -(\sigma_n + i(\Omega - 2\omega_n)/2)$, $\nu = i3\beta/2\omega_n$ and $\mu = -i/4\omega_n$.

The very same amplitude equation, originally derived by symmetry arguments, has been widely used for modelling the wave amplitude saturation of sub-harmonically unstable Faraday standing waves in lab-scale containers (see Douady (1990) and Henderson and Miles (1990) among many others). After fitting coefficients σ_n and β from experiments by Henderson and Miles (1990) of single-global-mode sub-harmonic Faraday waves in a small circular cylinder, approximation (1.16) is compared with those measurements in figure 1.7(b). The comparison is outlined in terms of the stability region associated with the sub-harmonic parametric resonance (grey-shaded area) and in terms of non-dimensional steady-state wave amplitude (large-time dynamics) at a fixed non-dimensional forcing amplitude.

Solid friction in free pendulum dynamics

The Duffing equation and the nonlinear Mathieu equation are examples of oscillatory dynamics which experience nonlinear effects for increasing amplitudes. Those effects are responsible for the saturation mechanism of the perturbation amplitude at large times. On the contrary, here we propose an example of nonlinearity becoming important for decreasing amplitudes and that is induced by dry friction in a simple pendulum initially perturbed out of its stable equilibrium position (Butikov, 2015):

$$\ddot{x} + 2\sigma_n \dot{x} + \omega_n^2 x + \Delta \operatorname{sgn} x = 0, \quad x(0) = x^i, \quad \dot{x}(0) = \dot{x}^i (= 0). \quad (1.17)$$

Assuming again small linear damping $\sigma_n = \epsilon \hat{\sigma}_n$ and small friction coefficient $\Delta = \epsilon \hat{\Delta}$, with $\hat{\sigma}_n$ and $\hat{\Delta}$ both of order $\sim O(1)$, an asymptotic approximation can be obtained in the form of an

1.2. Nonlinear effects and envelope equations

amplitude equation following Viola et al. (2018) and Dollet et al. (2020)

$$\boxed{\frac{dA}{dt} = \lambda A + \chi A / |A|}, \quad (1.18)$$

with $\lambda = -\sigma_n$ and $\chi = -\Delta/\pi\omega_n$.

Turning (1.18) into polar coordinates, $A = |A|e^{i\Phi}$, allows one to readily obtain an analytical solution for the envelope module of $x_0 = 2|A|\cos(\omega_n t + \Phi)$,

$$|A(t)| = \left[-\frac{\Delta}{\pi\sigma_n\omega_n} + \left(\frac{x_0}{2} + \frac{\Delta}{\pi\sigma_n\omega_n} \right) e^{-\sigma_n t} \right]. \quad (1.19)$$

Solution (1.19) suggests that the nonlinear term in (1.18) is such that there exist a finite time, $t = t^*$, for which the motion arrests irreversibly as $|A(t = t^*)|$ becomes zero,

$$t^* = \frac{1}{\sigma_n} \log \left(\frac{\pi\sigma_n\omega_n x_0 + 2\Delta}{2\Delta} \right), \quad (1.20)$$

a feature that has already been described in figure 1.6. This simple pendulum analogy can be used to model the nonlinear relaxation dynamics of small amplitude liquid oscillations induced by contact angle hysteresis (Dollet et al., 2020; Viola et al., 2018). In figure 1.7(c), after fitting coefficients σ_n and χ , the asymptotic prediction (1.19) is compared with the measurements by (Dollet et al., 2020) of the relaxation dynamics of liquid oscillations in a U-shaped tube and it is indeed shown to be in fairly good agreement.

1.2.2 Generalization to large systems: the emergence of secular terms and the imposition of a solvability condition via *Fredholm alternative*¹

In the previous section, by considering a few archetypal one-degree-of-freedom systems, we have discussed the asymptotic breakdown provoked by the emergence of secular terms in the straightforward weakly nonlinear expansion. Specifically, we have shown how the employment of the multiple time-scales method, by assuming a slow time amplitude modulation of the perturbation, naturally leads to the imposition of a solvability condition that eliminates secular terms and prescribes the perturbation amplitude to obey a given normal form, i.e. an amplitude equation.

In the following, we briefly discuss how the concepts of the emergence of secular terms and the imposition of a solvability condition are generalizable to large systems.

To this end, let us seek an asymptotic solution of, e.g., the Navier-Stokes equation (1.1) also subjected to an external and time-dependent body or boundary force, $\mathbf{f}(\mathbf{x}, t)$,

$$\mathbf{q}(\mathbf{x}, t) = \mathbf{q}_0(\mathbf{x}) + \epsilon \mathbf{q}_1(\mathbf{x}, t) + \epsilon^2 \mathbf{q}_2(\mathbf{x}, t) + \dots + \epsilon^k \mathbf{q}_k + O(\epsilon^{k+1}), \quad ||\mathbf{f}(\mathbf{x}, t)|| \sim \epsilon^k, \quad (1.21)$$

¹Part of these notes was kindly provided by Yves-Marie Ducimetière in personal communication.

Introduction

where \mathbf{q}_0 represents an equilibrium solution (or steady base flow) of (1.1) and where the amplitude of the external forcing $\|\mathbf{f}(\mathbf{x}, t)\|$ is assumed small of order ϵ^k . With the aim of giving a pedagogical example, in the following let us consider $k = 3$. After linearization of the governing equations around \mathbf{q}_0 , the ϵ -order problem generally takes the form of a linear homogeneous problem, such as

$$\frac{\partial \mathbf{q}_1}{\partial t} = \mathcal{L} \mathbf{q}_1. \quad (1.22)$$

As already discussed at the beginning of this introduction, one can then seek eigensolutions of (1.22) in the standard normal form

$$\mathbf{q}_1(\mathbf{x}, t) = A(T) \hat{\mathbf{q}}_{1n}(\mathbf{x}) e^{\lambda_n t} + c.c., \quad T = \epsilon^2 t, \quad (1.23)$$

where $\hat{\mathbf{q}}_{1n}$ is the n th eigenmode and λ_n is the corresponding eigenvalue, solution of the generalized eigenvalue problem

$$\lambda_n \hat{\mathbf{q}}_{1n} = \mathcal{L} \hat{\mathbf{q}}_{1n}. \quad (1.24)$$

The formalism of the multiple scales analysis requires the eigenvalue $\lambda_n = \sigma_n + i\omega_n$ to be marginally stable (Godrèche and Manneville, 1998). How to relax this constraint to cases where the growth or decay rate σ_n is much smaller than ω_n is discussed, e.g., in Meliga et al. (2009a). However, for the sake of simplicity, we assume hereinafter the marginal stability condition, i.e. $\sigma_n = 0$ and $\lambda_n = i\omega_n$. Note that, in the spirit of the multiple time-scales method, the perturbation amplitude $A(T)$ has been assumed to depend on the slow time scale T , as defined in (1.23); the use of the partial derivative symbol in (1.22) anticipated the decomposition of the physical time into two different time scales.

Before moving forward, let us also introduce an inner product, e.g. the Hermitian scalar product $\langle \hat{\mathbf{a}}, \hat{\mathbf{b}} \rangle = \hat{\mathbf{a}}^H \hat{\mathbf{b}}$, with $\hat{\mathbf{a}}$ and $\hat{\mathbf{b}}$ two generic vectors and the superscript H denoting the Hermitian transpose. With respect to the considered scalar product, we can define an adjoint operator of \mathcal{L} , namely \mathcal{L}^\dagger ,

$$\lambda_m^\dagger \hat{\mathbf{q}}_{1m}^\dagger = \mathcal{L}^\dagger \hat{\mathbf{q}}_{1m}^\dagger, \quad (1.25)$$

such that $\hat{\mathbf{q}}_{1m}^\dagger$ and λ_m^\dagger are, respectively, the m th adjoint eigenmode and adjoint eigenvalue. Particularly, the direct, $\hat{\mathbf{q}}_{1n}$ and adjoint, $\hat{\mathbf{q}}_{1m}^\dagger$, eigenmodes form a bi-orthogonal basis, meaning that $\langle \hat{\mathbf{q}}_{1m}^\dagger, \hat{\mathbf{q}}_{1n} \rangle = \delta_{nm}$, with δ_{nm} the Kronecker delta. Hence, for $n = m$, $\langle \hat{\mathbf{q}}_{1n}^\dagger, \hat{\mathbf{q}}_{1n} \rangle = 1$ and $\lambda_m^\dagger = \bar{\lambda}_n$ ($= -i\omega_n$ in the case here considered).

The problem at order ϵ^3 will typically take the form of an inhomogeneous linear problem, where the right-hand side contains forcing terms produced by the weakly nonlinear interactions of the previous order solutions and by the external body or boundary forces, e.g. a time-harmonic $\mathbf{f}(\mathbf{x}, t) = f \hat{\mathbf{f}}(\mathbf{x}) e^{i\Omega t} + c.c.$, whose amplitude f has been assumed to be small of order ϵ^3 and whose oscillation frequency is close to the natural frequency $\Omega \approx \omega_n$,

$$\frac{\partial \mathbf{q}_3}{\partial t} - \mathcal{L} \mathbf{q}_k = -\frac{\partial \mathbf{q}_1}{\partial T} + \mathcal{N}(\mathbf{q}_0, \mathbf{q}_1, \mathbf{q}_2, \dots) + \mathbf{f}(\mathbf{x}, t) = -\frac{\partial \mathbf{q}_1}{\partial T} + \mathcal{F}(A, f, \dots). \quad (1.26)$$

The forcing term $\mathcal{F}(A, f, \dots)$ is generally a function of the perturbation amplitude, forcing amplitude, etc. We also notice that the right-hand side contains a forcing term associated with

1.2. Nonlinear effects and envelope equations

the slow time derivative of the leading order perturbation \mathbf{q}_1 . Let us suppose now a Fourier decomposition of the time-dependent forcing term $\mathcal{F}(A, f, \dots)$ into a component gathering all the resonant terms oscillating at the natural frequency ω_n , $\mathcal{F}_{\text{RT}}(A, f, \dots)$ and a second component gathering all the non-resonant terms, $\mathcal{F}_{\text{NRT}}(A, f, \dots)$, which are not relevant for the further analysis and will be therefore simply ignored, so that (1.26) reduces to

$$\frac{\partial \mathbf{q}_k}{\partial t} = \mathcal{L} \mathbf{q}_k + \left(-\frac{\partial \mathbf{q}_1}{\partial T} + \mathcal{F}_{\text{RT}}(A, f, \dots) \right), \quad \mathcal{F}_{\text{RT}} = \hat{\mathcal{F}}(A, f, \dots) e^{i\omega_n t} + \text{c.c.}, \quad (1.27)$$

subjected to a certain initial condition, e.g. $\mathbf{q}_k = \mathbf{0}$ at $t = 0$.

In the most general form, the response of the system in time can be written by using the exponential matrix $e^{\mathcal{L}t}$, such that

$$\begin{aligned} \mathbf{q}_3(\mathbf{x}, t) &= e^{\mathcal{L}t} \int_0^t e^{-\mathcal{L}s} \left[\left(-\frac{\partial A}{\partial T} \hat{\mathbf{q}}_{1n} + \hat{\mathcal{F}}_{\text{RT}}(A, f, \dots) \right) e^{i\omega_n s} \right] ds = \\ &= \left(-\frac{\partial A}{\partial T} \hat{\mathbf{q}}_{1n} + \hat{\mathcal{F}}_{\text{RT}}(A, f, \dots) \right) e^{\mathcal{L}t} \int_0^t e^{-\mathcal{L}s} e^{i\omega_n s} ds + \text{c.c.}, \end{aligned} \quad (1.28)$$

The exponential matrix can be decomposed as

$$e^{\mathcal{L}s} = \mathcal{Q} e^{\mathcal{D}s} \mathcal{Q}^{-1}, \quad (1.29)$$

where the matrix \mathcal{Q} contains the eigenmodes of \mathcal{L} , whereas the diagonal matrix \mathcal{D} contains the corresponding eigenvalues of \mathcal{L} , i.e. $\mathcal{D} = \text{diag}\left(i\omega_n, -i\omega_n, \lambda_l, \bar{\lambda}_l, \dots\right)$ (with $l \neq n$). Hence,

$$e^{\mathcal{L}t} e^{-\mathcal{L}s} e^{i\omega_n s} = \text{diag}\left(e^{i\omega_n t}, e^{-i\omega_n(t-2s)}, e^{\lambda_l(t-s)+i\omega_n s}, e^{\bar{\lambda}_l(t-s)+i\omega_n s}, \dots\right), \quad (1.30)$$

Using the decomposition (1.29), one can express

$$\begin{aligned} &\int_0^t e^{\mathcal{L}t} e^{-\mathcal{L}s} e^{i\omega_n s} ds = \\ &= \mathcal{Q} \begin{bmatrix} te^{i\omega_n t} & 0 & 0 & 0 & \dots \\ 0 & \frac{1}{i2\omega_n} (e^{i\omega_n t} - e^{-i\omega_n t}) & 0 & 0 & \dots \\ 0 & 0 & \frac{1}{i\omega_n - \lambda_l} (e^{i\omega_n t} - e^{\lambda_l t}) & 0 & \dots \\ 0 & 0 & 0 & \frac{1}{i\omega_n - \bar{\lambda}_l} (e^{i\omega_n t} - e^{\bar{\lambda}_l t}) & \dots \\ \vdots & \vdots & \vdots & \vdots & \ddots \end{bmatrix} \mathcal{Q}^{-1}, \end{aligned} \quad (1.31)$$

so that,

$$\mathbf{q}_3 = \left(-\frac{\partial A}{\partial T} \hat{\mathbf{q}}_{1n} + \hat{\mathcal{F}}_{\text{RT}}(A, f, \dots) \right) \int_0^t e^{\mathcal{L}t} e^{-\mathcal{L}s} e^{i\omega_n s} ds + \text{c.c.} = \quad (1.32)$$

$$= \underbrace{\left(\hat{\mathbf{q}}_{1n} \frac{\langle \hat{\mathbf{q}}_{1n}^\dagger, \left(-\frac{\partial A}{\partial T} \hat{\mathbf{q}}_{1n} + \hat{\mathcal{F}}_{\text{RT}}(A, f, \dots) \right) \rangle}{\langle \hat{\mathbf{q}}_{1n}^\dagger, \hat{\mathbf{q}}_{1n} \rangle} e^{i\omega_n t} t + \text{c.c.} \right)}_{\text{secular terms: linearly growing in time } \propto t} + \text{oscillating}, \quad (1.33)$$

Introduction

in which we have used the fact that $\mathcal{Q} = (\hat{\mathbf{q}}_{1n}, \hat{\mathbf{q}}_{1m}, \dots)^T$ and, therefore,

$$\mathcal{Q}^{-1} \left(-\frac{\partial A}{\partial T} \hat{\mathbf{q}}_{1n} + \hat{\mathcal{F}}_{RT}(A, f, \dots) \right) = \begin{bmatrix} \frac{<\hat{\mathbf{q}}_{1n}^\dagger, (-\frac{\partial A}{\partial T} \hat{\mathbf{q}}_{1n} + \hat{\mathcal{F}}_{RT}(A, f, \dots))>}{<\hat{\mathbf{q}}_{1n}^\dagger, \hat{\mathbf{q}}_{1n}>} \\ \frac{<\hat{\mathbf{q}}_{1m}^\dagger, (-\frac{\partial A}{\partial T} \hat{\mathbf{q}}_{1n} + \hat{\mathcal{F}}_{RT}(A, f, \dots))>}{<\hat{\mathbf{q}}_{1m}^\dagger, \hat{\mathbf{q}}_{1m}>} \\ \vdots \end{bmatrix}, \quad (1.34)$$

since

$$\begin{aligned} \mathcal{Q} \mathcal{Q}^{-1} \left(-\frac{\partial A}{\partial T} \hat{\mathbf{q}}_{1n} + \hat{\mathcal{F}}_{RT}(A, f, \dots) \right) &= \sum_n \hat{\mathbf{q}}_{1n} \frac{<\hat{\mathbf{q}}_{1n}^\dagger, \left(-\frac{\partial A}{\partial T} \hat{\mathbf{q}}_{1n} + \hat{\mathcal{F}}_{RT}(A, f, \dots) \right)>}{<\hat{\mathbf{q}}_{1n}^\dagger, \hat{\mathbf{q}}_{1n}>} = \\ &= \left(-\frac{\partial A}{\partial T} \hat{\mathbf{q}}_{1n} + \hat{\mathcal{F}}_{RT}(A, f, \dots) \right), \end{aligned} \quad (1.35)$$

according to the bi-orthogonality property of direct and adjoint modes.

Lastly, from (1.32), it appears clear that avoiding an algebraic growth implies requiring that

$$\frac{<\hat{\mathbf{q}}_{1n}^\dagger, \left(-\frac{\partial A}{\partial T} \hat{\mathbf{q}}_{1n} + \hat{\mathcal{F}}_{RT}(A, f, \dots) \right)>}{<\hat{\mathbf{q}}_{1n}^\dagger, \hat{\mathbf{q}}_{1n}>} = 0. \quad (1.36)$$

which is equivalent to asking that the forcing term must be orthogonal to the cokernel of \mathcal{L} , or, alternatively said, to the kernel of the adjoint operator \mathcal{L}^\dagger , as stated by the *Fredholm alternative* (Olver, 2014a).

The imposition of a solvability condition through the *Fredholm alternative* eventually fixes the arbitrariness introduced by the perturbation amplitude by prescribing a governing equation for $A(T)$, which constitutes our final amplitude equation:

$$\frac{\partial A}{\partial T} = \frac{1}{\epsilon^2} \frac{dA}{dt} = \frac{<\hat{\mathbf{q}}_{1n}^\dagger, \hat{\mathcal{F}}_{RT}(A, f, \dots)>}{<\hat{\mathbf{q}}_{1n}^\dagger, \hat{\mathbf{q}}_{1n}>} \implies \boxed{\frac{dA}{dt} = F(A, f, \dots)} \quad (1.37)$$

As a side comment, we note that in our starting point (1.22), we have implicitly assumed that the mass matrix \mathcal{M} coincides with the identity matrix \mathcal{I} . In general, $\mathcal{M} \neq \mathcal{I}$ and \mathcal{M} enters in the definition of the inner product, $<\hat{\mathbf{a}}, \mathcal{M}\hat{\mathbf{b}}> = \hat{\mathbf{a}}^H(\mathcal{M}\hat{\mathbf{b}})$.

Lastly, it appears now clearer as the single-degree-of-freedom systems previously examined constitutes the trivial limit of equation (1.36). Indeed, by taking $\hat{\mathbf{q}}_{1n} = \hat{\mathbf{q}}_{1n}^\dagger = 1$, equation (1.36) simply means requiring that the resonant forcing terms are zero, i.e. $\frac{\partial A}{\partial T} - \hat{\mathcal{F}}_{RT}(A, f, \dots) = 0$.

1.2.3 In this thesis: derivation of normal form coefficients from first principles

In this section, we have introduced the multiple *time*-scale method, and we have illustrated, using a few single-degree-of-freedom archetypal examples, how to derive envelope equations for these systems. A generalization of the method to large systems has been then briefly discussed. Throughout this thesis, envelope equations (and their coefficients) for a series

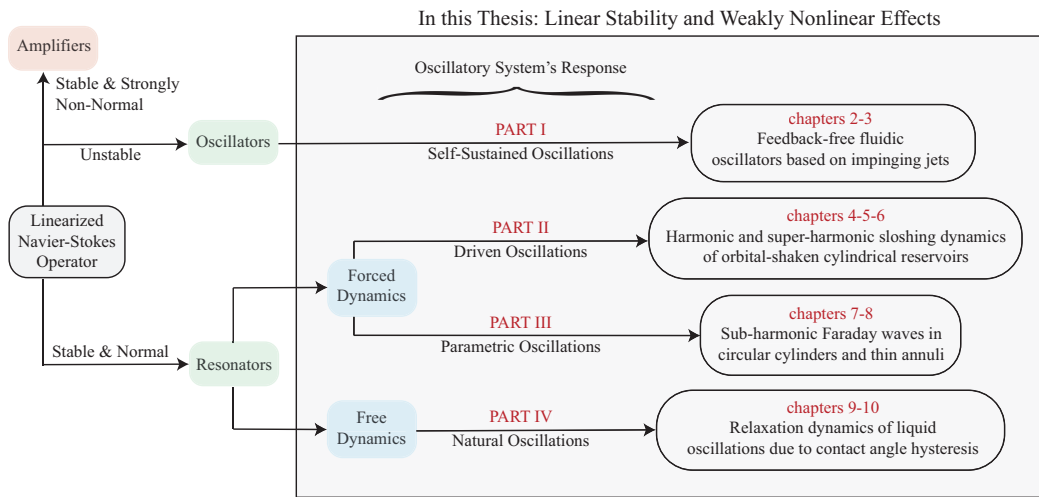


Figure 1.8 – Structure of the present document. This thesis is divided into four main parts, each classified according to the type of the underlying oscillatory system's response: self-sustained, externally driven, externally driven, but parametrically and natural. Each chapter is devoted to the theoretical modelling and further understanding of these complex nonlinear fluid dynamics using the tools of linear stability and weakly nonlinear theories.

of complex fluidic oscillators and resonators will be formally derived (and computed) from first principles via weakly nonlinear multiple time-scales analyses of the full hydrodynamic systems. It will be shown that the weakly nonlinear dynamics of these oscillatory flows, ranging from self-sustained impinging-jets oscillators to driven sloshing-like resonator, is well described by slightly different and enriched versions of the envelope equations just introduced, i.e. (1.4), (1.13), (1.16) and (1.18), hence making possible the identification of the few degrees-of-freedom that are actually relevant to the overall dynamics.

1.3 Forewords

Despite the main focus on fundamental physics questions, the problems tackled in this thesis are directly relevant to several industrial applications. While in many engineering problems, as those of figure 1.1(b,d,f), oscillatory instabilities and resonances are seen as endangering features to be avoided at all costs, resulting in entire parametric regions to be avoided or in the need for efficient control and mitigation strategies, the examples discussed in this document, like many others, illustrate a different view: self-sustained or driven oscillations can be indeed harnessed for the design of a wide variety of engineering devices, ranging from microfluidic circuitry (hydrodynamic converters or switching devices), orbital-shaken bioreactors for cell cultivation and drug production to liquid-based template for the assembly of microscale materials. A proper predictive understanding and modelling of the hydrodynamic at stake is therefore essential in the design of all these processes.

With the support of existing and home-made experimental observations and measurements (see figure 1.9), the present research aims precisely at modelling and providing comprehensive

Introduction

theoretical frameworks capable of rationalising some of these complex nonlinear oscillatory dynamics, most of which have not been fully elucidated yet.

As amplifier-like systems have not been studied in this thesis, let us recall the distinction made between oscillators and resonators on the basis of the nature of their oscillatory responses:

- Oscillators:
 - **Self-sustained oscillations**
- Resonators:
 - **Driven oscillations**
 - **Parametric oscillations**
 - **Natural oscillations**

Keeping in mind the distinction made above, the present document is organised as in figure 1.8 and figure 1.9. The thesis contains published or submitted material carried out in collaboration with other experienced researchers and my supervisor, to which I fundamentally contributed. If a Chapter contains published material where I do not appear as the first author, my personal contribution is explicitly specified at the beginning of the Chapter.

In the following, a general outline of this thesis with a short description of each part is provided, whereas more detailed and dedicated introductions are given at the beginning of each part.

PART I *Self-sustained oscillations*

Chapters 2-3: Feedback-free fluidic oscillators based on impinging jets

In **Chapter 2**, we describe a microfluidic oscillator based on facing impinging jets and operating in laminar flow conditions. Using appropriate cross-junction configurations with two intersecting inlets and outlets, pulsatile liquid flows are experimentally generated at the microscale from steady and equal inlet flow conditions and without moving parts or external stimuli. Experiments and DNS are used to determine the region in the control parameter space (device's geometry and Reynolds number, Re) where self-sustained oscillations manifest.

To better elucidate the physical mechanism behind these oscillations, in **Chapter 3**, we consider a simplified two-dimensional configuration. Advances in the understanding of such a mechanism are made by performing linear global stability and sensitivity analysis, which identify the Kelvin–Helmholtz instability, located in the jet's interaction region, as the main candidate for the origin of the oscillations observed in fluidic devices. Further interesting nonlinear flow features, involving symmetry-breaking and subcritical transitions, are also described by means of the weakly nonlinear theory.

PART II *Driven oscillations***Chapter 4-5-6: Harmonic and super-harmonic sloshing dynamics of orbital-shaken cylindrical reservoirs**

The container motion along a planar circular trajectory at a constant angular velocity, i.e. *circular shaking*, is of interest in several industrial applications, e.g. for fermentation processes or in the cultivation of stem cells, where good mixing and efficient gas exchange are the main targets. Under this external forcing condition, the system always responds with a swirling wave co-directed with the container's direction of motion. Depending on the driving frequency and amplitude, the frequency response can be either harmonic or super-harmonic. In **Chapter 4**, existing experimental data are used to develop a weakly nonlinear model capable of describing the fundamental harmonic and super-harmonic resonances in terms of flow patterns and amplitude response.

From the perspective of hydrodynamic instability, the case of longitudinal container motions, i.e. *longitudinal shaking*, appears more interesting. In this configuration, the system exhibits a richer variety of wave regimes, such as planar, irregular and swirling motions. In **Chapter 5**, we extend the weakly nonlinear model previously developed in order to study harmonic and super-harmonic resonances under these forcing conditions. Our theoretical predictions are confirmed by dedicated experiments.

Lastly, in **Chapter 6**, with the main focus on harmonic resonances, we provide an experimental characterisation of the free liquid surface response for a generic, elliptic periodic container trajectory, i.e. *elliptical shaking*, so as to bridge the gap between the two diametrically opposed shaking conditions previously discussed. Experiments demonstrate for the first time the counter-intuitive existence of stable swirling waves travelling in the opposite direction of the container motion. These findings are then rationalized by using a slight variation of the theoretical tools developed in Chapters 4 and 5.

PART III *Parametric oscillations***Chapter 7-8: Sub-harmonic Faraday waves in circular cylinders and thin annuli**

In this Part, we consider the problem of Faraday waves, undoubtedly the most famous parametric resonator system in fluids. In particular, we tackle two very different system configurations, but which are linked to each other for the importance of the lateral wall and contact line boundary conditions.

In **Chapter 7**, we focus on the problem of the coupling and interaction of parametric waves and capillary meniscus waves, the latter being typically unwanted. Their suppression of the latter can be achieved by imposing a contact line pinned at the container brim. However, tunable meniscus waves are desired in some applications such as those of liquid-based biosensors, where they can be controlled by adjusting the shape of the static meniscus by slightly under/overfilling the vessel while keeping the contact line fixed at the brim. Considering this contact line condition in cylindrical containers, we formalize a weakly nonlinear analysis

Introduction

which predicts the impact of static contact angle effects on the instability onset of viscous sub-harmonic Faraday waves. The theory is validated with previous experiments and DNS.

In **Chapter 8** we instead consider the case of Faraday waves in Hele-Shaw cells, for which previous theoretical analyses typically rely on the Darcy approximation based on the parabolic flow profile assumption in the narrow direction. However, Darcy's model is known to be inaccurate whenever inertia is not negligible, e.g. in unsteady flows. In this work, we propose a revised gap-averaged linear model that accounts for inertial effects induced by the unsteady terms in the Navier-Stokes equations. The theory also includes a linear law for the dynamic contact angle that serves to reintroduce the contact line dissipation. The latter is indeed seen to be a critical contribution to the overall dissipation of the system. The stability of the system is studied by performing a Floquet analysis, whose predictions compare well with previous experiments in rectangular Hele-Shaw cells and with new dedicated experiments in thin annuli.

PART IV Natural oscillations

Chapter 9-10: Nonlinear relaxation dynamics of free surface oscillations due to contact angle hysteresis

In **Chapter 9**, we present a physics-inspired mathematical model based on successive linear eigenmode projections to solve the relaxation (natural dynamics) of small-amplitude and two-dimensional viscous capillary-gravity waves with a phenomenological and experimentally-inspired nonlinear contact line model accounting for Coulomb solid-like friction. We show that each projection eventually induces a rapid loss of total energy in the liquid motion and contributes to its nonlinear damping. This approach captures the transition from a contact line stick-slip (or nearly stick-slip) motion to a pinned (or nearly pinned) configuration, as well as the secondary fluid bulk motion following the arrest of the contact line, overlooked by previous asymptotic analyses.

In **Chapter 10**, the projection model formalized in Chapter 9 is applied to the more realistic case of liquid oscillation in a U-tube configuration. A comparison with existing experiments proves the predictive power of this method, although a fitting parameter is still required owing to the lack of information about the actual contact line dynamics.

See figure 1.9 for a visual illustration of the salient points pertaining to each Part.

1.3. Forewords

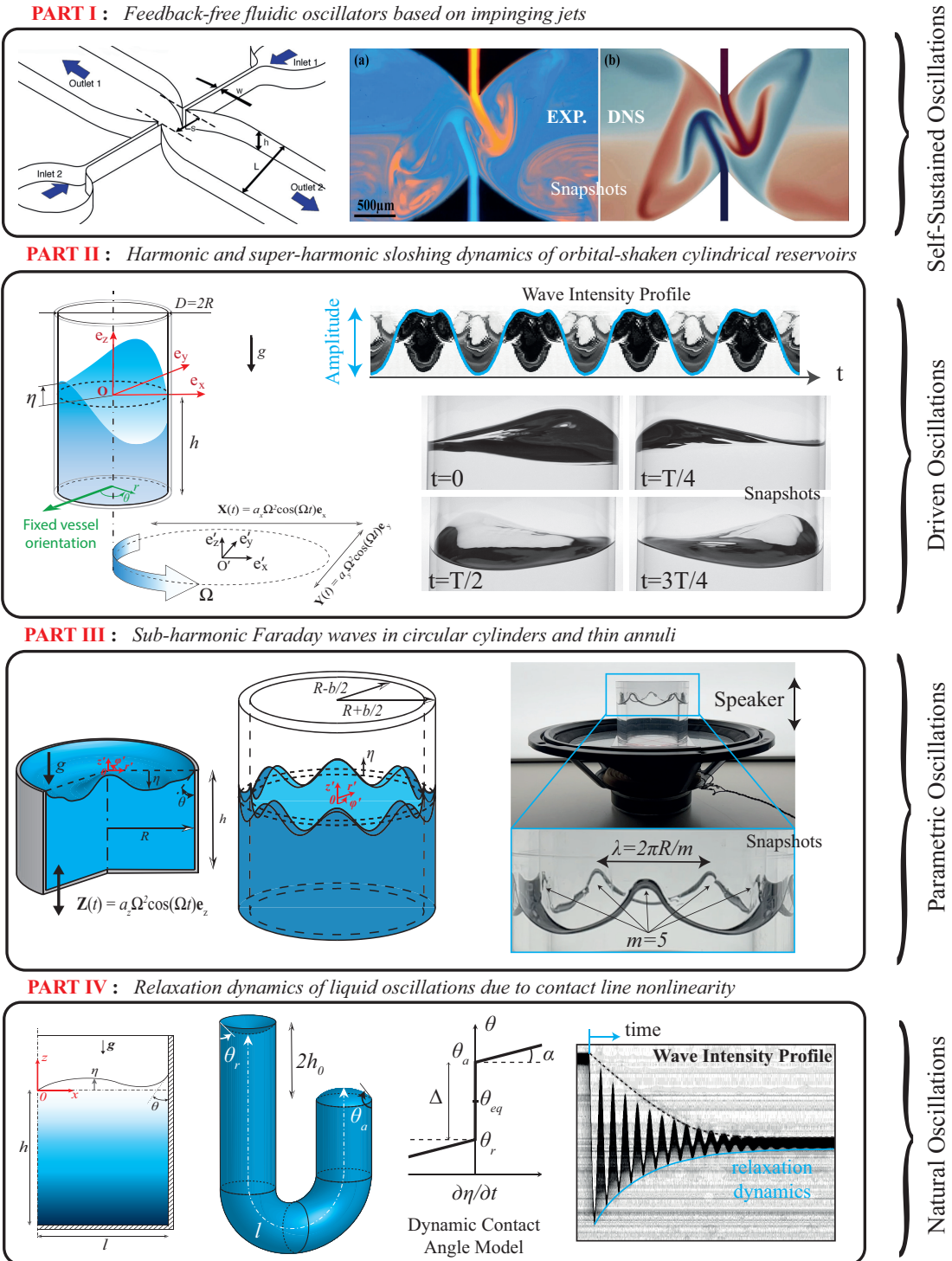


Figure 1.9 – Visual illustration of the salient points pertaining to the main Parts of this thesis. The classification is based on the nature of the fluid oscillations. Sketches, representing the various geometrical configurations considered, are given on the right, whereas a few examples of homemade experimental outputs are given on the left. Theoretical models have been built on the basis of these observations.